ACS APPLIED MATERIALS & INTERFACES

RESEARCH ARTICLE

www.acsami.org

Poly(aniline) Nanowires in Sol−Gel Coated ITO: A pH-Responsive Substrate for Planar Supported Lipid Bilayers

Chenhao Ge, Kristina S. Orosz, Neal R. Armstrong, and S. Scott Saavedra*

Department of Chemistry and Biochemistry, University of Arizona, Tucson, Arizona 85721-0041, United States

Supporting Information

ABSTRACT: Facilitated ion transport across an artificial lipid bilayer coupled to a solid substrate is a function common to several types of bioelectronic devices based on supported membranes, including biomimetic fuel cells and ion channel biosensors. Described here is fabrication of a pH-sensitive transducer composed of a porous sol−gel layer derivatized with poly(aniline) (PANI) nanowires grown from an underlying planar indium−tin oxide (ITO) electrode. The upper sol−gel surface is hydrophilic, smooth, and compatible with deposition of a planar supported lipid bilayer (PSLB) formed via vesicle fusion. Conducting tip AFM was used to show that the PANI wires are connected to the ITO, which convert this electrode into a potentiometric pH sensor. The response to changes in the pH of the buffer contacting the PANI nanowire/sol−gel/ITO electrode is blocked by the very low ion permeability of the overlying fluid PSLB. The feasibility of using this assembly to monitor facilitated proton transport across the PSLB was demonstrated by doping the membrane with lipophilic ionophores that respond to a transmembrane pH gradient, which produced an apparent proton permeability several orders of magnitude greater than values measured for undoped lipid bilayers.

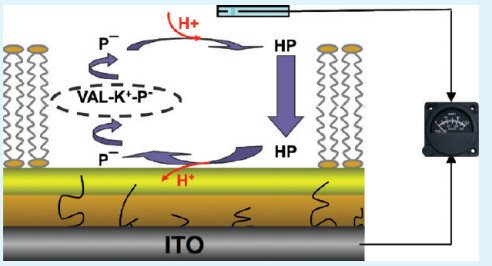

KEYWORDS: lipid bilayer, proton transport, sol−gel, poly(aniline), conductive tip AFM, nanowires, indium−tin oxide, ionophore

INTRODUCTION

Facilitated ion transport across a lipid membrane is a fundamental process in biological energy transduction,[1−3] and creation of artificial lipid bilayers that mediate transmembrane ion flux underlies the development of several types of bioelectronic devices, including biosensors and biomimetic fuel cells.[4−9] Facilitated transmembrane ion transport has been most frequently studied using vesicles.[1,8,10−12] Notable examples include (1) an artificial photosynthetic system that uses a photogenerated, transmembrane proton gradient to drive ATP synthesis,[10,12] and (2) proton pumping by integral membrane proteins across a lipid bilayer coated on a mesoporous silica particle.[13,14] Vesicular assemblies, however, are not readily interfaced to a physical transducer to provide a direct electrical readout. Ion-responsive optical probes confined to the vesicle interior are typically used to detect transmembrane ion gradients.

Membrane−transducer integration can be accomplished by coupling a planar lipid bilayer to a solid electrode.[9] Numerous types of lipid bilayer architectures supported on a variety of planar electrode materials, including Au, doped Si, and indium−tin oxide (ITO), have been prepared and characterized (e.g., refs 9,15−18 and references therein). Coupling the membrane to an electrode allows transmembrane ion transport to be monitored electrochemically, usually using voltammetry, potentiometry, or impedance spectroscopy. Planar lipid bilayer/electrode assemblies have been used as hosts for ionophores, ion channels, and proton pumping proteins such as cytochrome oxidase.[19−24] For example, Steinem and co-workers used nanoporous electrodes coated with planar bilayers to support the proton-pumping activity of incorporated bacteriorhodopsin.[25] These and other examples suggest the potential for "wiring" a planar membrane to substrate electrode to allow use of the transmembrane potential gradient to drive a coupled electrochemical process.

Optical detection of transmembrane proton transport across planar lipid membranes using either fluorescence or absorbance detection has also been reported.[26,27] When the membrane assembly is supported on an optically transparent electrode such as indium−tin oxide (ITO), both optical and electrochemical methods can be combined in a complementary manner.[26,28,29] For example, McBee et al.[26] deposited a planar bilayer on a self-assembled film of poly(aniline) (PANI) and poly(acrylic acid) (PAA) that was coated on an ITO electrode. A redox-active proton shuttle was used to couple electron and proton transport across the membrane. Proton transport was detected as a change in the visible absorbance of the PANI film using planar waveguide attenuated total reflection (ATR) spectroscopy. In this construct, however, the adhesion of the membrane to the PANI/PAA film was very weak, resulting in frequent defect formation and consequent ion leakage across the membrane. This paper describes an improved approach for coupling a planar bilayer to ITO that has been modified with PANI to make it sensitive to proton activity.

PANI is a pH-sensitive conducting polymer that has been widely utilized as a sensor transducer.[29−35] It is typically deposited onto electrodes using electrochemical polymerization or

Received: April 13, 2011
Accepted: June 14, 2011
Published: June 14, 2011

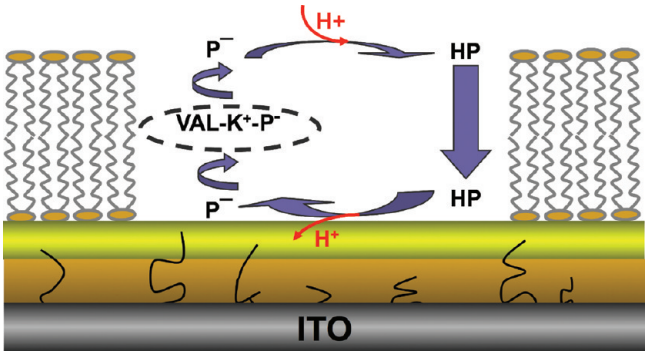

Figure 1. Schematic diagram of two porous sol−gel glass layers coated on a planar ITO electrode. PANI nanowires are electrochemically polymerized from the ITO surface through the pores of the lower sol−gel layer. A planar supported lipid bilayer (PSLB) is deposited on the upper sol−gel layer. Valinomycin, an ionophore, and CCCP, a protonophore, are dissolved in the PSLB, where P^-, HP, and VAL represent deprotonated CCCP, protonated CCCP, and valinomycin, respectively. A transmembrane pH gradient drives transmembrane proton transport via HP/P^- and aided by VAL. This process decreases the pH below the PSLB, which is detected as a change in the potential of the PANI/sol−gel/ITO electrode.

adsorption from solution; however, a PANI coating is not a suitable surface for deposition of a lipid bilayer by vesicle fusion.[26] An interpenetrating network of a conducting polymer in a porous sol−gel glass offers an alternative.[36] The sol−gel not only provides a mechanically stable matrix for polymer incorporation, but also adheres well to ITO and other types of electrode materials[36−38] and is compatible with vesicle fusion.[39,40] PANI can be synthesized within sol−gels by first allowing the aniline monomers to diffuse into the porous glass network, followed by electrochemical polymerization,[41,42] or by premixing the monomers with the sol−gel precursor solution, followed by deposition onto an electrode and subsequent electrochemical polymerization.[36,43] The latter strategy was employed here to prepare a sol−gel layer on ITO functionalized with PANI nanoelectrodes. A second thinner sol−gel layer was then applied to create a smooth hydrophilic surface suitable for deposition of a planar supported lipid bilayer (PSLB) by vesicle fusion. The overall structure of the supramolecular assembly, which incorporates ionophores into the membrane, is shown in Figure 1. The feasibility of using this PANI nanoelectrode/sol−gel hybrid layer to monitor ionophore-facilitated proton transport across the PSLB was demonstrated.

EXPERIMENTAL SECTION

Reagents. The following chemicals were purchased from Aldrich and used without further purification: tetraethyl orthosilicate (TEOS), 99.999%; methyltriethoxysilane (MTES), 99%; valinomycin, 98.0%; and carbonyl cyanide 3-chlorophenylhydrazone (CCCP), 98.0%. Aniline (Aldrich, 99.5%) was distilled before use. Deionized (DI) water was obtained from a Barnstead Nanopure system with a measured resistivity of 18.0 MΩ·cm or higher. L-α-phosphatidylcholine (egg, chicken) (egg PC), and 1-palmitoyl-2-[6-[(7-nitro-2-1,3-benzoxadiazol-4-yl)amino]-hexanoyl]-*sn*-glycero-3-phosphocholine (NBD-PC) were obtained from Avanti Polar Lipids.

ITO Substrates. Polished soda lime glass, 1 mm thick, coated with ITO, was purchased from Applied Films Corporation. The sheet resistance was ≤20 Ω per square, and the thickness of the ITO layer was about 84 nm with a refractive index of 1.91 (measured by ellipsometry with a Sentech SE 400 ellipsometer at 633 nm at a reflection angle of 70°). ITO substrates were cleaned by gently scrubbing with a cotton pad soaked with Alconox, then rinsing with DI water. Substrates were then sonicated in ethanol for 15 min, blown dry with nitrogen, and cleaned in an air plasma (Harrick model PDC-3XG) for 5 min at 15 W. Cleaned substrates were used immediately upon removal from the plasma cleaner.

Aniline Doped Sol−Gel Layer Preparation. Sol−gel layers doped with aniline were prepared from a precursor solution consisting of 1.8 mL of TEOS, 0.2 mL of MTES, 600 μL of ethanol, 2 μL of aniline, and 646 μL of 43 mM HCl as the catalyst. This solution was vigorously stirred in the dark for 6 h at room temperature to yield a clear liquid. Within the ensuing 1 h, the precursor solution was diluted 1:1 (v/v) with methanol, then passed through a 0.45 μm syringe filter and spun cast onto cleaned ITO substrates at 3000 rpm for 1 min. This process was performed in air at 10−15% relative humidity (RH). The coated electrodes were cured in the dark at room temperature at approximately 15−20% RH for 48 h prior to electrochemical polymerization of the entrapped aniline.

Electrochemical Polymerization. Cyclic voltammetry (CV) was performed utilizing an EG&G potentiostat (PAR, model 263A). The electrochemical cell consisted of an ITO working electrode coated with a sol−gel layer with an exposed surface area of 0.8 cm^2, a Ag/AgCl reference electrode (Bioanalytical Systems), and a platinum wire counter electrode. Electrochemical polymerization of aniline entrapped in the sol−gel layer was performed by scanning the potential from −0.4 to 1.2 V at a rate of 50 mV/s with the sol−gel/ITO electrode immersed in 0.1 M acetate buffer, pH 4.5. After electrochemical polymerization, sol−gel/ITO electrodes were cured at room temperature at 15−20% RH for 2 days.

Deposition of Sol−Gel Capping Layer on PANI-Doped Sol−Gel/ITO Electrodes. Sol−gel capping layers were prepared from a precursor solution containing 4 mL of TEOS, 1.2 mL of ethanol, 1.244 mL of DI H_2O, and 48 μL of 0.25 M HCl. This solution was vigorously stirred for 6 h, mixed with 1.2 mL of ethanol and 7.692 mL of methanol, and used within the subsequent 1 h. Deposition of this solution on sol−gel/ITO electrodes was performed by dip coating at a withdrawal rate of 17 cm/min. Just prior to deposition, sol−gel/ITO electrodes were treated in a low temperature air plasma for 5 s under low power to generate a hydrophilic surface. The electrodes coated with two sol−gel layers were cured at room temperature at 15−20% RH for at least 36 h and then rehydrated in 10 mM buffer solution (pH 3 or pH 6) overnight prior to further experimentation.

PSLB Deposition. To prepare small unilamellar vesicles (SUVs) for vesicle fusion, an appropriate amount of egg PC dissolved in chloroform, or NBD-PC mixed with egg PC at a 5:95 molar ratio, was added into a cleaned glass vial and dried under an Ar stream, followed by drying under vacuum for 4 h. The lipids were then resuspended in 10 mM pH 7 phosphate buffer at a final concentration of 0.5 mg/mL, followed by vortexing for 30 s, and then sonicating at 25 °C in a Branson sonicator fitted with a cup horn until the solution turned clear. The SUV solution was then injected into the cell containing the sol−gel coated ITO electrode. Vesicle fusion was allowed to proceed for 30 min, after which unfused vesicles were rinsed out with phosphate buffer.

Analytical and Physical Characterization. CV and potentiometry were used to characterize the electrochemical properties of PANI-doped sol−gel/ITO electrodes. Potentiometric measurements were performed using a pH meter (Denver Instruments, model 215) with ±0.1 mV measurement accuracy and 6×10^{12} Ω input impedance. The steady state potential of coated electrodes was measured after an equilibration time of 5 min in a series of 10 mM buffers containing 50 mM KCl. The buffer components and pH values were phosphate (pH 3, 6, 7, and 8), acetate (pH 4, 5), and borate (pH 9).

Tapping mode atomic force microscopy (AFM) was performed on a Dimension 3100 Nanoscope IV system (Veeco) in air. Tapping mode

etched silicon probes with a nominal force constant of 42 N/m and device frequency of about 320 kHz were used. Conducting tip AFM measurements were performed using a Dimension 3100 Nanoscope IV system with a tunneling AFM (TUNA) application module. A diamond-like carbon-coated Si tip with a nominal force constant of 2.8 N/m (DDESP, Veeco) was mounted onto an electrical cantilever holder and coupled to the TUNA module through a sample bias pin. Measurements were performed in contact mode in air, with application of a minimal initial force to engage the tip, followed by incrementally raising the force. Both height and current images were generated and recorded simultaneously upon the application of an appropriate sample bias. Water contact angle measurements were performed using a Kruss Drop Shape Analysis (DSA 10Mk2) instrument at ambient temperature and humidity.

Fluorescence imaging and fluorescence recovery after photobleaching (FRAP) measurements on PSLBs were performed using a Nikon Eclipse TE2000-U microscope. For FRAP, PSLBs composed of egg PC (the blank) or NBD-PC/egg PC (the sample) were formed in the two compartments of a liquid cell. PSLBs on glass microscope slides (Gold Seal Products #3010; cleaned in Piranha solution for 30 min and rinsed thoroughly with DI water before use) were used as a reference for PSLBs on sol−gel coated ITO.

RESULTS AND DISCUSSION

Aniline Electropolymerization in Sol−Gel Layers on ITO. The electropolymerization of aniline was performed using CV. Panel (a) of Figure 2 shows a CV recorded with an aniline loading density of 3.4 mM in the sol−gel layer. The potential sweep, initiated at −400 mV, shows very little faradaic current until approximately 500 mV, where a sharp increase in the anodic current indicates the initiation of aniline oxidation and polymerization. The polymerization current reaches a maximum around 735 mV and then declines, which is likely due to the diffusion limit of aniline in the sol−gel pores. During the subsequent cathodic scan, a large peak centered at about 196 mV is assigned to the reduction of the PANI formed during the anodic scan.

The redox activity of electrochemically polymerized PANI was then examined. Panel (b) of Figure 2 shows a CV of a PANI-doped sol−gel layer in 0.1 M pH 4.5 acetate buffer. To prevent polymerization of the residual aniline monomer, the potential sweep range was restricted to −400 mV to 500 mV. One pair of redox reaction peaks was observed, with a midpoint potential of 224 mV and a peak-to-peak separation of 40 mV, showing that the PANI is electrically connected to the underlying ITO. These results are in qualitative agreement with those reported by Cihaner and co-workers.[44] In a mixed water/organic solvent electrolyte, aniline can only be partially oxidized to the EB/ES form on the electrode surface. Consequently, only one pair of redox peaks is observed. The nonzero peak separation is consistent with expectations for a PANI redox reaction that is limited by the diffusion of counterions and solvent in the pores of the sol−gel network.

AFM Characterization of PANI-Doped Sol−Gel Layers on ITO. AFM characterization (Figure 3a) shows that the surface of a cleaned ITO electrode is relatively rough with a rms surface roughness of approximately 1.4−2 nm. Deposition of a sol−gel layer can generate a smoother surface. The layer thickness after aging in dark for 2 days was about 300 nm (Table 1). A typical AFM image of a sol−gel layer on ITO prior to PANI formation is shown in panel (b) of Figure 3. The film surface is relatively smooth with a rms surface roughness of about 0.4 nm over a 10 μm × 10 μm scan area. Occasional pinholes were observed

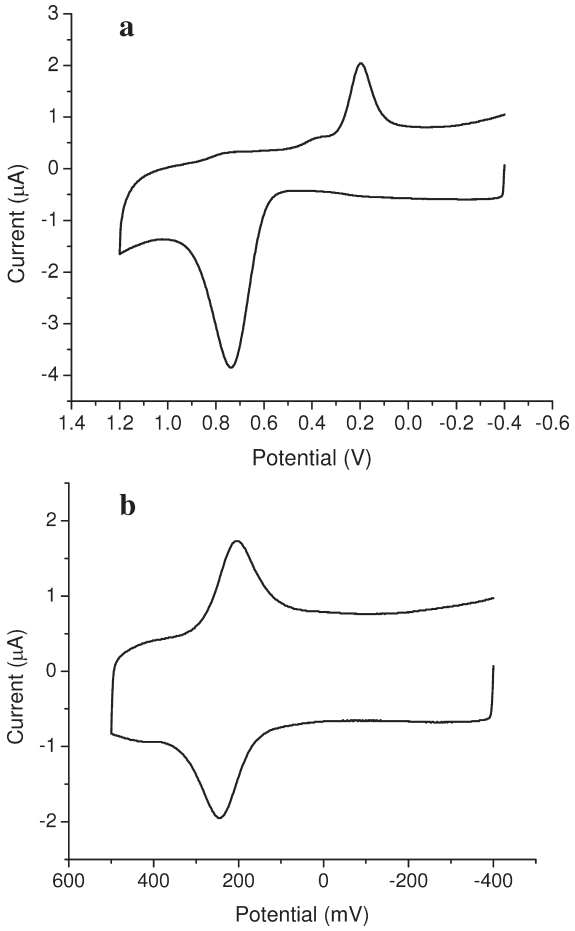

Figure 2. (a) Initial cyclic voltammogram of a sol−gel layer doped with aniline (3.4 mM loading density) and coated on an ITO electrode in 0.1 M acetate buffer at a scan rate of 50 mV/s. The onset potential of aniline polymerization is around 500 mV. (b) Cyclic voltammogram of a sol−gel layer containing electrochemically polymerized PANI on an ITO electrode in 0.1 M acetate buffer, pH 4.5, at a 50 mV/s scan rate.

that likely arose from rapid solvent evaporation during spin coating. After electrochemical polymerization, PANI nanoelectrodes emerged from the pores of sol−gel. Typical AFM images are shown in panels (c) and (d) of Figure 3. Because the surface of the sol−gel layer prior to PANI growth was relatively smooth and featureless, all of the features shown as white particles (in the height image, Figure 3c) or protrusions (in the 3D image, Figure 3d) are considered to be PANI nanoelectrodes.

To further confirm that these features are PANI in electrical contact with the ITO electrode, a conducting tip AFM (C-AFM) study was performed. C-AFM can map simultaneously the topography and conductivity of a surface with high spatial resolution and has been applied to characterization of molecular junctions and their electrical properties down to the nanometer scale.[45−47] To enhance the resolution, a thinner sol−gel layer (80 nm thick) doped with 2.8 mM aniline was prepared and electropolymerized. The C-AFM height image and corresponding current image of this sample are shown in panels (a) and (b) of Figure 4, respectively. The correlation between the locations of the surface protrusions (Figure 4a) and the areas of relatively higher current (Figure 4b) is clear. This is strong evidence that the surface protrusions are PANI nanoelectrodes that are in electrical contact with the underlying ITO electrode.

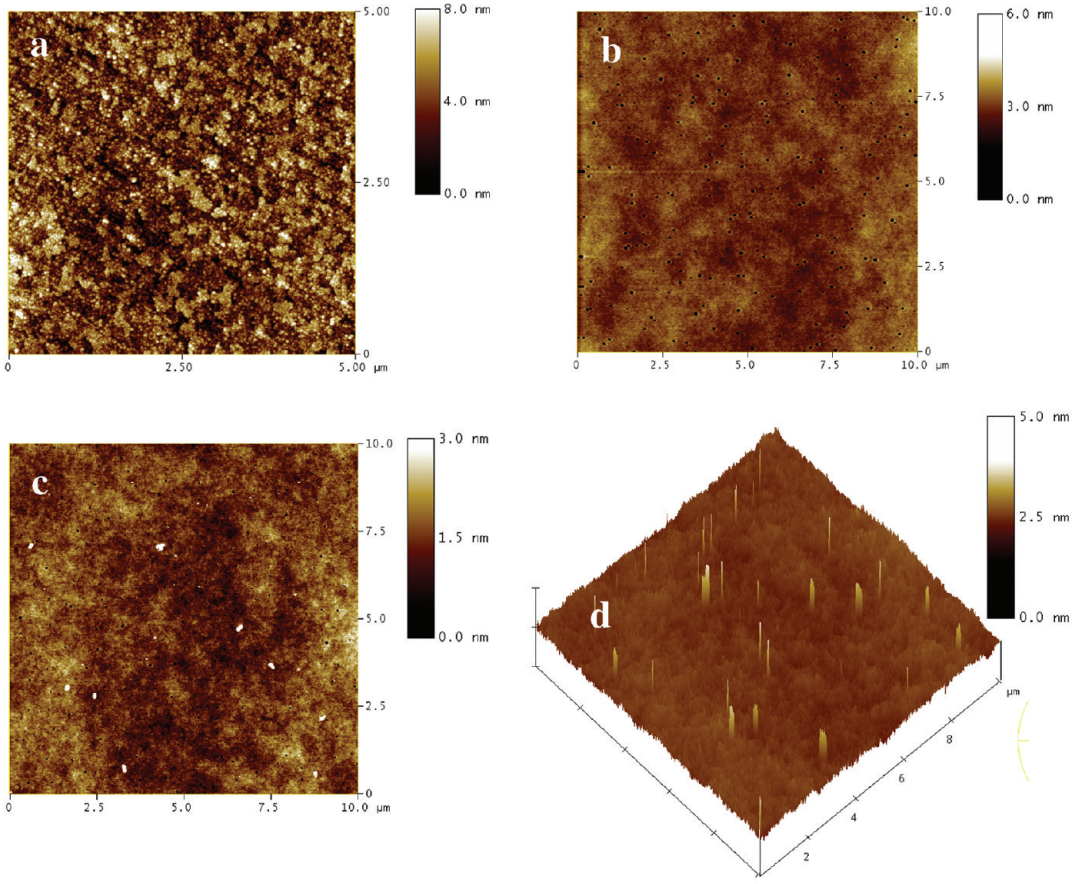

Figure 3. Tapping mode AFM height images of (a) the surface of a cleaned ITO electrode; (b) a sol−gel layer doped with aniline on an ITO electrode, prior to aniline polymerization; and (c) a sol−gel/ITO electrode after electrochemical polymerization of aniline. (d) Three-dimensional image of the surface shown in panel (c). The scan areas are 5 μm × 5 μm in panel (a) and 10 μm × 10 μm in panels (b−d).

Table 1. Static Water Contact Angle and Film Thickness Analysis of PANI-Doped Sol−Gel/ITO Electrodes before and after Deposition of a TEOS Capping Layer

substrate	contact angle before rehydration (deg)[a]	contact angle after rehydration (deg)[a]	film thickness[a] (nm)
PANI-doped sol−gel/ITO electrode	59 ± 1.1	14 ± 1.3	297 ± 3.3
CL/PANI/sol−gel/ITO electrode	47 ± 0.9	<5	402 ± 1.9[b]

[a] n = 5. [b] The thickness of the capping layer, obtained by difference, was 105 ± 2.6 nm.

Potentiometric Measurements of PANI Nanoelectrodes as pH Transducers. The potentiometric behavior of PANI-doped sol−gel/ITO electrodes to changes in buffer pH was studied. To remove the organic solvent and residual aniline in the sol−gel layer as well as rehydrate it, electrodes were soaked in 10 mM pH 3 phosphate buffer overnight before use. Figure 5 shows a typical potentiometric response curve to changes in pH. A pseudo-Nernstian response with a slope of 48 mV/pH was observed over pH 3−9. The response time was typically less than 2 min.

The 48 mV/pH slope is less than the value of about 57 mV/pH measured for self-assembled PANI/PAA films on ITO.[29] A lower slope is expected for PANI entrapped in a sol−gel glass because the high number density of silanol groups in the pores makes the solvent in the pores more acidic than the bulk solvent in contact with the glass.[48] pH changes in the pores that result from changes in the bulk pH will consequently be buffered by the silanol groups, which are much more numerous than the basic sites on PANI (Supporting Information). The wide dynamic range of the pH response in Figure 5 is expected. The close proximity of silanols in the pores, as well as heterogeneities in the surface chemistry and morphology of the pores, should produce a broad distribution of chemically inequivalent sites and a correspondingly broad response to changes in bulk pH, as observed for other types of sol−gel pH sensors.[49,50] Furthermore, PANI is a polyelectrolyte containing both amine and imine groups. The proximity of these groups in the polymer chains and differences in their local chemical environment (e.g., due to variations in chain packing in the pores) should further broaden the distribution of inequivalent basic sites.[29,33,51,52]

In previous papers,[26,29,53] we showed that the pH response of self-assembled PANI/PAA films on ITO could be monitored using visible ATR spectroscopy on a multimode planar waveguide. It was not possible to use this approach here because the surface coverage of the PANI wires in the sol−gel/ITO electrodes

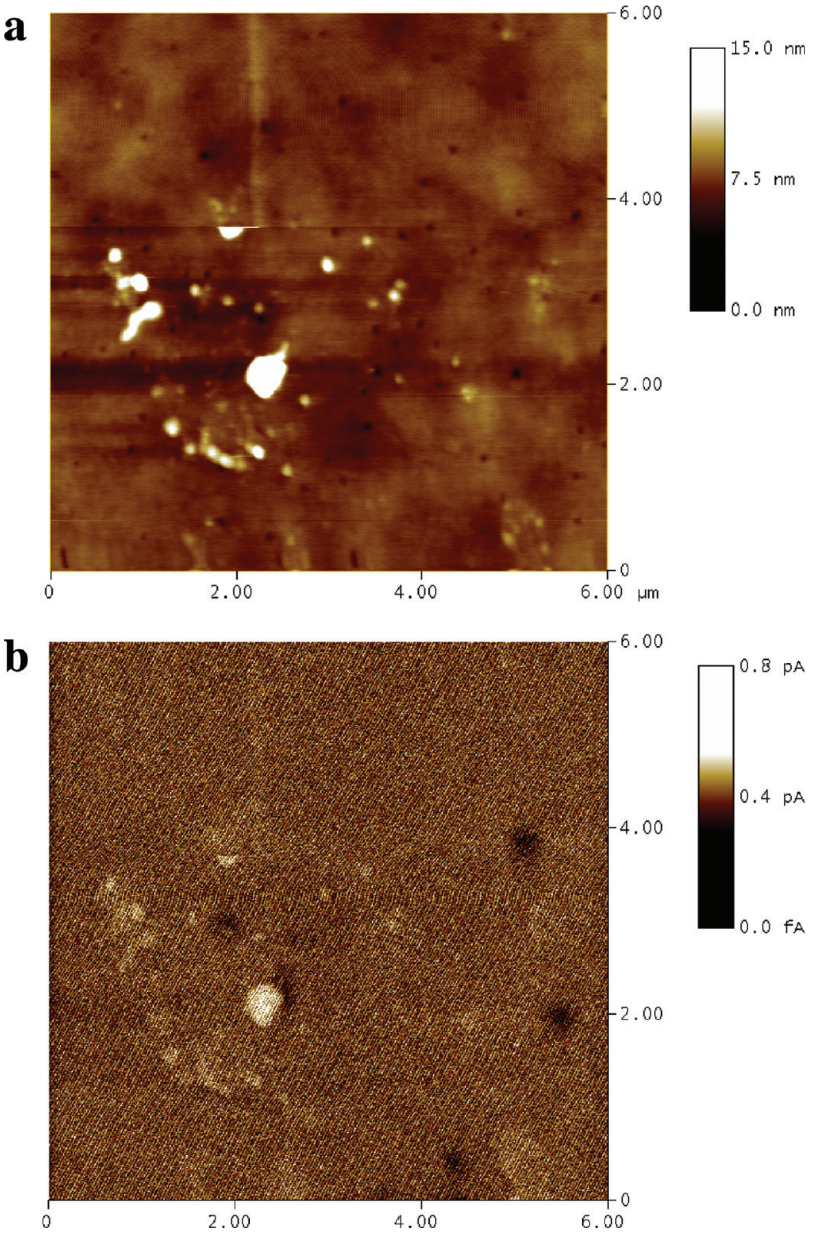

Figure 4. C-AFM height image (a) and current image (b) of a sol−gel/ITO electrode containing electropolymerized PANI. Scan area is 6 μm × 6 μm.

was much lower than that of PANI in the self-assembled films studied in the earlier work. The requisite sensitivity could be achieved by using a much thinner electroactive waveguide.[54]

Sol−Gel Capping Layer Deposition and Characterization. As shown in panels (c) and (d) of Figure 3, the PANI nanoelectrodes protrude from the sol−gel layer. These protrusions increase the roughness and the hydrophobicity of surface. To form a continuous, uniform PSLB by vesicle fusion, a hydrophilic substrate surface with low surface roughness is usually required.[55,56] To generate a surface more compatible with PSLB deposition, a TEOS capping layer was deposited on PANI-doped sol−gel/ITO electrodes by dip-coating. After aging for 2 days at room temperature in ambient atmosphere, the measured thickness of the capping layer was about 105 nm (Table 1). A representative AFM image (Figure 6a) of this multilayer structure, denoted CL/PANI/sol−gel/ITO, shows that the surface is featureless and relatively smooth, with a rms surface roughness of about 0.3 nm. Comparing this image to those in Figure 3, it is clear that the PANI protrusions have been encapsulated in the TEOS matrix.

Static water contact angle measurements were performed to characterize the surface hydrophilicity. The results are summarized in Table 1. Prior to rehydration overnight in 10 mM pH 3 phosphate buffer, the surface before and after the capping layer deposition was moderately hydrophobic, with values of 55° and 47°, respectively. After rehydration, the contact angle on both surfaces declined significantly to 14° and <5°, respectively. These decreases are likely due to leaching of organic byproducts and unreacted aniline from the porous sol−gel layers. The lower contact angle of the capping layer surface is attributed to the different compositions of the sol−gel layers. The lower layer contains methyl groups due to the use of MTES as a precursor and PANI protrusions; both components should increase surface hydrophobicity. In contrast, the capping layer is fabricated from TEOS, and the encapsulated PANI does not protrude from its upper surface.

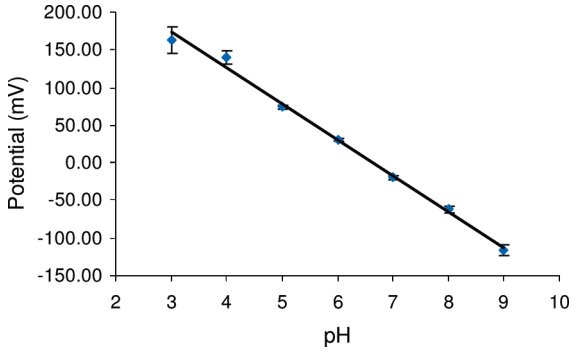

Figure 5. Potentiometric response as a function of pH from 3 to 9 of a PANI-doped sol−gel/ITO electrode. Measurements were made after a 5 min equilibration time at each pH. The slope is 48 mV/pH over the pH range of 3−9 (R^2 = 0.9947). The error bars represent the standard deviation of three measurements at each pH.

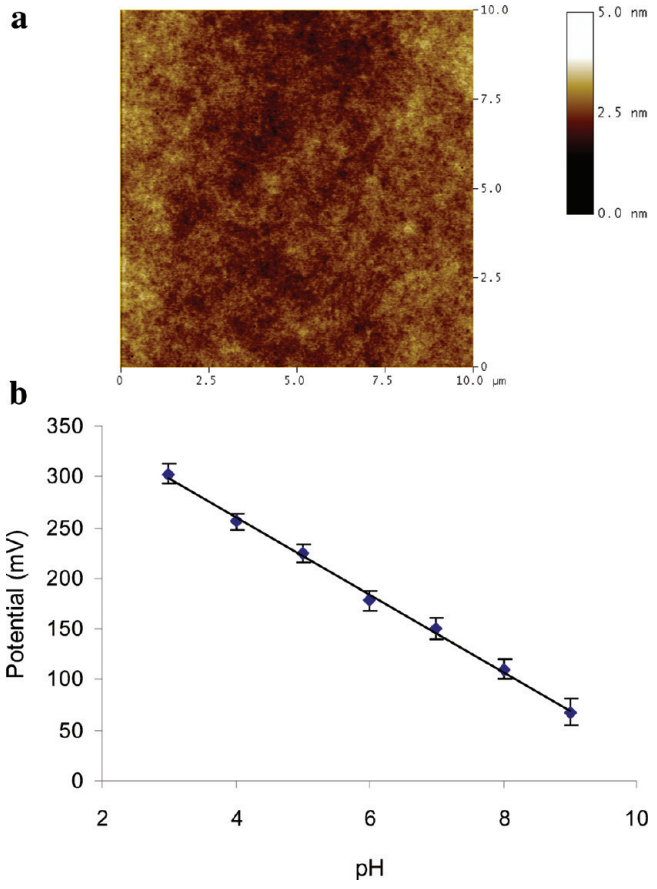

Figure 6. (a) Tapping mode AFM height image of a CL/PANI/sol−gel/ITO electrode (scan areas is 10 μm × 10 μm). The rms surface roughness is about 0.30 nm. (b) Potentiometric response as a function of pH from 3 to 9 of a CL/PANI/sol−gel/ITO electrode. Measurements were made after a 5 min equilibration time at each pH. The slope is 38 mV/pH over the pH range of 3−9 (R^2 = 0.9975). Error bars represent the standard deviation of three measurements at each pH.

The potentiometric behavior of CL/PANI/sol−gel/ITO electrodes to changes in buffer pH after overnight rehydration was examined. A typical potentiometric response curve is shown in panel (b) of Figure 6. A pseudo-Nernstian response with a slope of 38 mV/pH was observed over pH 3−9 with a response time typically less than 2 min. This result demonstrates that the capping layer is porous, allowing the encapsulated PANI nanoelectrodes to retain their pH sensing properties, although the slope of the response is lower than the value of 48 mV/pH measured before deposition of the capping layer. This decrease is expected because the PANI wires are now fully encapsulated in the acidic sol−gel pores.

PSLB Deposition and Characterization. Egg PC vesicles containing NBD-PC were fused on CL/PANI/sol−gel/ITO electrodes. After rinsing unfused vesicles from the surface, epifluorescence microscopy showed a featureless luminescent image (data not shown), demonstrating the uniformity of the PSLB on the micrometer length scale. FRAP was used to examine the lateral mobility of the lipids in fused bilayers. Figure S-1 in the Supporting Information shows a set of epifluorescence images of a PSLB composed of egg PC doped with NBD-PC deposited on a CL/PANI/sol−gel/ITO electrode. The recovery of the photobleached spot is consistent with the presence of a PSLB in which NBD-PC has long-range lateral mobility.

Quantitative measurements of lateral lipid diffusion were performed, using glass as a reference substrate. Typical FRAP curves measured for PSLBs deposited on glass slides and CL/PANI/sol−gel/ITO electrodes are shown in Figure S-2 of the Supporting Information. The respective diffusion coefficients, D, were 3.0 ± 0.4 $\mu m^2/s$ and 2.7 ± 0.2 $\mu m^2/s$, with percent recoveries of 96 ± 3.4% and 92 ± 7.6%. The observation of significant mobility of lipids on CL/PANI/sol−gel/ITO electrodes shows that these lipid films are laterally continuous and are not composed predominately of adsorbed vesicles (for which the percent recovery would be minimal).[57]

Proton Permeability of PSLBs on CL/PANI/Sol−Gel/ITO Electrodes. Studies of proton permeability across egg PC PSLBs on CL/PANI/sol−gel/ITO electrodes were performed. In these experiments, the pH of the buffer above the PSLB was changed, and the temporal potentiometric response of the underlying electrode was measured. A typical result is shown in Figure S-3 of the Supporting Information when the buffer pH was changed from 7 to 6. The measured potential was very stable with less than a 2 mV variation within 1 h, indicating the pH gradient across the lipid membrane was maintained. In comparison, the data in panel (b) of Figure 6 show that in absence of a PSLB, the electrode potential shifts rapidly by about 38 mV. These data show that the defect density in the PSLB was low, otherwise the gradient would have decayed rapidly after the change in buffer pH.

The net proton−hydroxyl flux across a lipid membrane is dependent on the pH gradient.[58,59] The proton−hydroxyl flux, J_{net}, is given by[60]

$$J_{net} = P_{net} \times \Delta C \quad (3)$$

where P_{net} is the net proton−hydroxyl permeability coefficient ($P_{net} = P_{OH^-} + P_{H^+}$, where P_{OH^-} and P_{H^+} are the permeability coefficients of hydroxide ions and protons, respectively), and ΔC is the proton activity difference across the membrane. The permeability coefficients of protons and hydroxide ions are relatively high, with the majority of published values in the range of 10^{-3} to 10^{-6} cm/s;[58,59] in contrast, the permeability coefficients of sodium and potassium are much lower, in the range of 10^{-12} to 10^{-14} cm/s.[58] However, when the pH gradient across the membrane is small, the rate at which it dissipates will be slow.[59] This is the case for the experimental result shown in Figure S-3 of the Supporting Information; ΔC is small so

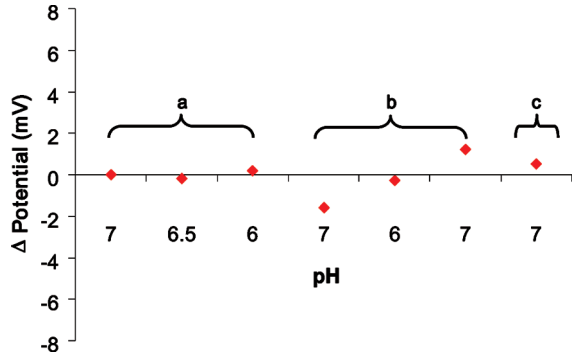

Figure 7. Potentiometric response of a CL/PANI/sol−gel/ITO electrode coated with a PSLB was monitored to assess the barrier properties of the membrane during exposure to a variety of experimental conditions. (a) The pH of the buffer above the PSLB was changed from 7 to 6.5, then to 6, and finally back to 7. (b) Valinomycin solution was injected into the flow cell and allowed to partition into the PSLB. The cell was then flushed with pH 7 buffer. The pH of the buffer above the PSLB was changed from 7 to 6 and then back to 7. (c) CCCP solution was injected into the flow cel, allowed to partition into the PSLB, and then the cell was flushed with pH 7 buffer. In all cases, the cell potential was measured 5 min after each injection of fresh buffer.

dissipation of the pH gradient across the bilayer is negligible on a time scale of hours.

Ionophore-Mediated Transmembrane Proton Transport. Transmembrane proton transport aided by lipophilic ionophores was examined to further characterize the pH sensing properties of these multilayer assemblies. Valinomycin, a K^+ ionophore, and CCCP, a protonophore, were inserted into PSLBs on CL/PANI/sol−gel/ITO electrodes to measure ΔpH-driven proton transport. Ionophore-mediated transmembrane proton transport using valinomycin and CCCP has been studied in liposomes,[61,62] and the proton transport mechanism has been described by Ahmed and Krishnamoorthy.[62−64] The proposed mechanism, illustrated in Figure 1, involves cotransport of K^+ in the opposite direction to counter the charge imbalance generated by proton transport. To our knowledge, valinomycin/CCCP-mediated proton transport across lipid bilayers has only been studied using liposomes.

The behavior of each component of the molecular assembly (Figure 1) was tested individually during each experiment to ensure the proper functioning of the entire assembly, as follows: (1) The pH response of the CL/PANI/sol−gel/ITO electrode was tested before PSLB deposition. Typically, a near Nernstian response with a slope of 38 mV/pH unit was observed (Figure 6b). (2) The barrier properties of the PSLB were tested as described above. Typically, the variation in cell potential was less than 2 mV when the pH of the buffer above the PSLB was changed, as shown in section (a) of Figure 7. (3) Six mL of valinomycin solution (2 μM in 10 mM pH 7 buffer with 50 mM KCl) was then injected into the flow cell. Because of its high lipid/water partition coefficient ($K_{l/w} \approx 5 \times 10^4$),[58] the valinomycin will preferentially insert into the PSLB. The potentiometric response to pH changes was tested again. As shown in section (b) of Figure 7, the cell potential remained stable through changes in pH from 7 to 6, and then back to 7. Therefore, the barrier properties of the PSLB were not altered by valinomycin insertion. (4) Six mL of CCCP solution (20 μM in 10 mM pH 7 buffer with 50 mM KCl) was then injected into the flow cell. Like valinomycin, the lipophilicity of CCCP

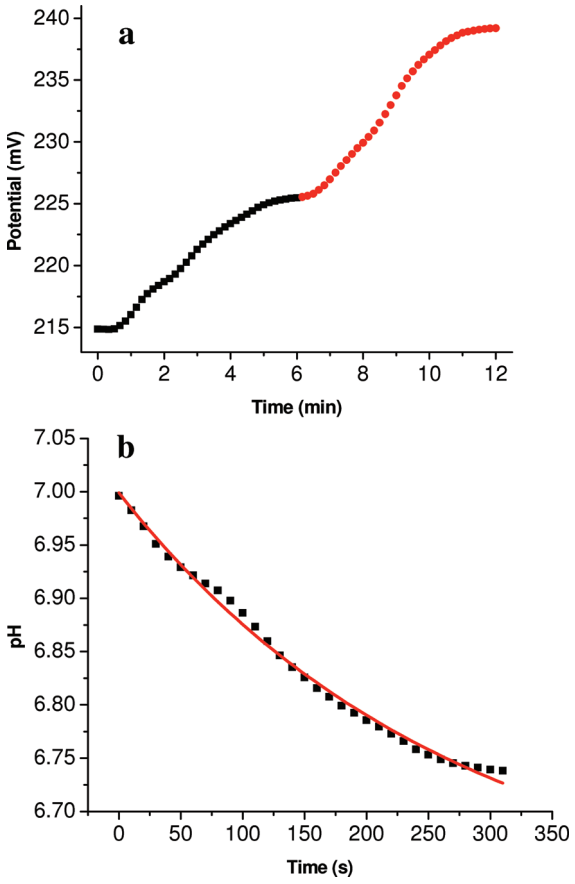

Figure 8. (a) Potentiometric response of a CL/PANI/sol−gel/ITO electrode coated with a PSLB containing CCCP and valinomycin. After equilibration at pH 7, buffers of pH 6.5 and 6 were injected into the flow cell at $t = 0$ and $t = 6$ min, respectively. The squares (■) and the circles (red filled circles) show the change in cell potential during the change from 7 to 6.5 and from 6.5 to 6, respectively. (b) The potential data in panel (a) from 40 to 360 s were converted to pH using a calibration curve measured for an electrode lacking a PSLB (Figure 6b) and plotted vs time. Because of the slow rate of buffer injection into the flow cell, the electrochemical cell potential in panel (a) did not start to change until about 40 s after the injection was initiated. Therefore, the *x*-axis values in panel (b) were adjusted such that 0 s is equivalent to 40 s on the *x*-axis in panel (a). The solid line is a first order exponential fit of the data to eq 4.

($K_{l/w} = 2.8 \times 10^4$)[65,66] causes it to preferentially insert into the PSLB. The cell potential remained stable during CCCP injection and subsequent flushing of the flow cell with pH 7 buffer, showing that the barrier properties of the membrane were not altered by CCCP insertion (section c of Figure 7). At then end of this sequence, ΔpH-driven proton transport across the PSLB was initiated.

Panel (a) of Figure 8 shows a typical time-dependent potentiometric response of the electrode when the pH of the buffer in the flow cell was changed from 7 to 6.5 and then to 6. A significant increase in cell potential occurred, consistent with protonation of the PANI nanoelectrodes beneath the PSLB due to ionophore-mediated transmembrane transport. The time-dependent potentiometric response curve was converted into a temporal pH response curve using the calibration curve obtained for electrodes lacking PSLBs (Figure 6b). In panel (b) of Figure 8, the ΔpH relaxation data are plotted for the buffer change from pH 7 to 6.5. A similar curve was observed for the pH change from 6.5 to 6 (data not shown).

A small pH gradient across a lipid bilayer should decay according to[58]

$$\Delta pH(t) = \Delta pH(t = 0) \times exp(-t/\tau) \quad (4)$$

where t is the time, τ is the lifetime, and ΔpH is the pH difference across the bilayer. For the planar assembly shown in Figure 1, $\Delta pH = pH_u - pH_a$ where the subscripts u and a refer to below and above the PSLB, respectively. The change in pH below the PSLB per unit time can be expressed as[58]

$$\frac{dpH_u}{dt} = J_{net}\frac{A}{VB} \quad (5)$$

where V is the aqueous volume below the PSLB, $B = -(d[H^+]/dpH)$ is the buffer capacity in that volume, and A is the PSLB surface area; eqs 3−5 allow calculation of J_{net} and P_{net} from the experimental data.

The data in panel (b) of Figure 8 were fit to a single exponential decay from which τ = 270 s and $(dpH_u)/(dt) = 1.85 \times 10^{-3}\ s^{-1}$ were obtained. Using calculated and measured values for V, B, and A (Supporting Information), the apparent P_{net} of the PSLB containing valinomycin and CCCP was calculated to be 0.4 $cm \cdot s^{-1}$ (see the Supporting Information for details). This value is about 10^3−10^6 times greater than P_{net} values measured near pH 7 for bilayers lacking ionophores.[58−60,67] This experiment and the results obtained from it are representative of several experiments carried out using independently prepared CL/PANI/sol−gel/ITO electrodes coated with PSLBs. Overall these results demonstrate that ITO coated with a hybrid sol−gel/PANI/PSLB multilayer functions as a transducer to detect proton transport across the lipid bilayer.

CONCLUSION

In a previous study,[26] we deposited a PANI/PAA self-assembled multilayer on ITO to create a pH-sensitive coating that supported vesicle fusion to form a PSLB. However, the PANI/PAA multilayer did not effectively planarize the very rough surface ITO surface , and adhesion of the lipid bilayer was weak. These problems caused frequent formation of proton-permeable defects in the PSLB. In the present study, a new type of planar lipid bilayer/electrode assembly designed to detect transmembrane proton transport was prepared and characterized. A porous sol−gel layer was used to template polymerization of PANI nanoelectrodes from an underlying ITO electrode, and the C-AFM and electrochemical data demonstrate that these electrodes are in electrical contact with the ITO surface. PANI derivatization converted the ITO electrode to a potentiometric pH sensor with a wide dynamic range. Applying the sol−gel capping layer buried the nanoelectrodes and planarized the electrode surface. The sol−gel glass surface is also compatible with deposition of a continuous fluid PSLB, whereas ITO is not. The elimination of the pH response after PSLB deposition shows that the bilayer is continuous and largely free of proton-permeable defects. Finally, PSLB/CL/PANI/sol−gel/ITO electrodes were functionalized with lipophilic ionophores, and a pH gradient was used to drive proton transport across the membrane. The apparent proton permeability was several orders of magnitude greater than that of pure lipid bilayers, demonstrating the feasibility of using this multilayer assembly to monitor transmembrane proton transport. The PSLB/CL/PANI/sol−gel/ITO assembly should be useful in future studies of more complex proton transporters such as proton pumping proteins.

ASSOCIATED CONTENT

Supporting Information. Calculation of ionophore-mediated proton permeability of PSLBs on CL/PANI-sol−gel/ITO electrodes, FRAP data, and pH response of a CL/PANI-sol-gel/ITO electrode coated with a PSLB. This information is available free of charge via the Internet at http://pubs.acs.org.

AUTHOR INFORMATION

Corresponding Author

*E-mail: saavedra@u.arizona.edu. Phone: 520-621-9761. Fax: 520-621-8407.

ACKNOWLEDGMENT

During its initial stages, this work was partially supported by the National Science Foundation under Grant CHE-0518702. The latter stages of this work were partially funded by the National Institutes of Health, National Institute of Biomedical Imaging and Bioengineering, under Grant R01EB007047. Any opinions, findings, and conclusions or recommendations expressed herein are those of the authors and do not necessarily reflect the views of the National Science Foundation, the National Institute of Biomedical Imaging and Bioengineering, or the National Institutes of Health. C.G. gratefully acknowledges partial support from a fellowship from Merck Research Laboratories and a fellowship from the Proposition 301 Initiative on Photonics, Arizona Board of Regents.

REFERENCES

(1) Robinson, J. N.; Cole-Hamilton, D. J. *Chem. Soc. Rev.* **1991**, *20*, 49–94.
(2) Brzezinski, P. *Trends Biochem. Sci.* **2004**, *29*, 380–387.
(3) Hambourger, M.; Moore, G. F.; Kramer, D. M.; Gust, D.; Moore, A. L.; Moore, T. A. *Chem. Soc. Rev.* **2009**, *38*, 25–35.
(4) Goc, J.; Hara, M.; Tateishi, T.; Miyake, J. *J. Photochem. Photobiol., A* **1996**, *93*, 137–144.
(5) Gust, D.; Moore, T. A.; Moore, A. L. *Acc. Chem. Res.* **2001**, *34*, 40–48.
(6) Cornell, B. A.; BraachMaksvytis, V. L. B.; King, L. G.; Osman, P. D. J.; Raguse, B.; Wieczorek, L.; Pace, R. J. *Nature* **1997**, *387*, 580–583.
(7) Tien, H. T.; Salamon, Z.; Ottova, A. *Crit. Rev. Biomed. Eng.* **1991**, *18*, 323–340.
(8) Luo, T. J. M.; Soong, R.; Lan, E.; Dunn, B.; Montemagno, C. *Nat. Mater.* **2005**, *4*, 220–224.
(9) Tanaka, M.; Sackmann, E. *Nature* **2005**, *437*, 656–663.
(10) Steinberg-Yfrach, G.; Rigaud, J. L.; Durantini, E. N.; Moore, A. L.; Gust, D.; Moore, T. A. *Nature* **1998**, *392*, 479–482.
(11) Khairutdinov, R. F.; Hurst, J. K. *Nature* **1999**, *402*, 509–511.
(12) Steinberg-Yfrach, G.; Liddell, P. A.; Hung, S. C.; Moore, A. L.; Gust, D.; Moore, T. A. *Nature* **1997**, *385*, 239–241.
(13) Davis, R. W.; Flores, A.; Barrick, T. A.; Cox, J. M.; Brozik, S. M.; Lopez, G. P.; Brozik, J. A. *Langmuir* **2007**, *23*, 3864–3872.
(14) Nordlund, G.; Ng, J. B. S.; Bergstrom, L.; Brzezinski, P. *ACS Nano* **2009**, *3*, 2639–2646.
(15) Naumann, R.; Schiller, S. M.; Giess, F.; Grohe, B.; Hartman, K. B.; Karcher, I.; Koper, I.; Lubben, J.; Vasilev, K.; Knoll, W. *Langmuir* **2003**, *19*, 5435–5443.
(16) Naumann, R.; Walz, D.; Schiller, S. M.; Knoll, W. *J. Electroanal. Chem.* **2003**, *550*, 241–252.
(17) Hillebrandt, H.; Wiegand, G.; Tanaka, M.; Sackmann, E. *Langmuir* **1999**, *15*, 8451–8459.
(18) Atanasov, V.; Knorr, N.; Duran, R. S.; Ingebrandt, S.; Offenhausser, A.; Knoll, W.; Koper, I. *Biophys. J.* **2005**, *89*, 1780–1788.

(19) Naumann, R.; Schmidt, E. K.; Jonczyk, A.; Fendler, K.; Kadenbach, B.; Liebermann, T.; Offenhäusser, A.; Knoll, W. *Biosens. Bioelectron.* **1999**, *14*, 651–662.
(20) Burgess, J. D.; Rhoten, M. C.; Hawkridge, F. M. *Langmuir* **1998**, *14*, 2467–2475.
(21) Naumann, R.; Baumgart, T.; Graber, P.; Jonczyk, A.; Offenhausser, A.; Knoll, W. *Biosens. Bioelectron.* **2002**, *17*, 25–34.
(22) Jeuken, L. J. C.; Bushby, R. J.; Evans, S. D. *Electrochem. Commun.* **2007**, *9*, 610–614.
(23) Vockenroth, I. K.; Atanasova, P. P.; Jenkins, A. T. A.; Koper, I. *Langmuir* **2008**, *24*, 496–502.
(24) McGillivray, D. J.; Valincius, G.; Heinrich, F.; Robertson, J. W. F.; Vanderah, D. J.; Febo-Ayala, W.; Ignatjev, I.; Losche, M.; Kasianowicz, J. J. *Biophys. J.* **2009**, *96*, 1547–1553.
(25) Schmitt, E. K.; Nurnabi, M.; Bushby, R. J.; Steinem, C. *Soft Matter* **2008**, *4*, 250–253.
(26) McBee, T. W.; Wang, L. Y.; Ge, C. H.; Beam, B. M.; Moore, A. L.; Gust, D.; Moore, T. A.; Armstrong, N. R.; Saavedra, S. S. *J. Am. Chem. Soc.* **2006**, *128*, 2184–2185.
(27) Yang, T. H.; Yee, C. K.; Amweg, M. L.; Singh, S.; Kendall, E. L.; Dattelbaum, A. M.; Shreve, A. P.; Brinker, C. J.; Parikh, A. N. *Nano Lett.* **2007**, *7*, 2446–2451.
(28) Hillebrandt, H.; Tanaka, M.; Sackmann, E. *J. Phys. Chem. B* **2002**, *106*, 477–486.
(29) Ge, C.; Armstrong, N. R.; Saavedra, S. S. *Anal. Chem.* **2007**, *79*, 1401–1410.
(30) Agbor, N. E.; Petty, M. C.; Monkman, A. P. *Sens. Actuators, B* **1995**, *28*, 173–179.
(31) Karyakin, A. A.; Vuki, M.; Lukachova, L. V.; Karyakina, E. E.; Orlov, A. V.; Karpachova, G. P.; Wang, J. *Anal. Chem.* **1999**, *71*, 2534–2540.
(32) Sangodkar, H.; Sukeerthi, S.; Srinivasa, R. S.; Lal, R.; Contractor, A. Q. *Anal. Chem.* **1996**, *68*, 779–783.
(33) Pringsheim, E.; Terpetschnig, E.; Wolfbeis, O. S. *Anal. Chim. Acta* **1997**, *357*, 247–252.
(34) Lindfors, T.; Ivaska, A. J. *Electroanal. Chem.* **2002**, *531*, 43–52.
(35) Lindino, C. A.; Bulhoes, L. O. S. *Anal. Chim. Acta* **1996**, *334*, 317–322.
(36) Doherty, W. J.; Armstrong, N. R.; Saavedra, S. S. *Chem. Mater.* **2005**, *17*, 3652–3660.
(37) Walcarius, A.; Mandler, D.; Cox, J. A.; Collinson, M.; Lev, O. *J. Mater. Chem.* **2005**, *15*, 3663–3689.
(38) Lev, O.; Wu, Z.; Bharathi, S.; Glezer, V.; Modestov, A.; Gun, J.; Rabinovich, L.; Sampath, S. *Chem. Mater.* **1997**, *9*, 2354–2375.
(39) Weng, K. C.; Stalgren, J. J. R.; Risbud, S. H.; Frank, C. W. *J. Non-Cryst. Solids* **2004**, *350*, 46–53.
(40) Mendes, S. B.; Bradshaw, J. T.; Saavedra, S. S. *Appl. Opt.* **2004**, *43*, 70–78.
(41) das Neves, S.; de Torresi, S. I. C.; Zoppi, R. A. *Synth. Met.* **1999**, *101*, 754–755.
(42) Verghese, M. M.; Ramanathan, K.; Ashraf, S. M.; Kamalasanan, M. N.; Malhotra, B. D. *Chem. Mater.* **1996**, *8*, 822–824.
(43) Widera, J.; Cox, J. A. *Electrochem. Commun.* **2002**, *4*, 118–122.
(44) Cihaner, A.; Onal, A. M. *Polym. Int.* **2002**, *51*, 680–686.
(45) Liau, Y. H.; Scherer, N. F.; Rhodes, K. *J. Phys. Chem. B* **2001**, *105*, 3282–3288.
(46) Lin, H. N.; Chen, S. H.; Perng, G. Y.; Chen, S. A. *J. Appl. Phys.* **2001**, *89*, 3976–3979.
(47) Wold, D. J.; Haag, R.; Rampi, M. A.; Frisbie, C. D. *J. Phys. Chem. B* **2002**, *106*, 2813–2816.
(48) Dunn, B.; Zink, J. I. *Chem. Mater.* **1997**, *9*, 2280–2291.
(49) Lee, J. E.; Saavedra, S. S. *Anal. Chim. Acta* **1994**, *285*, 265–269.
(50) Yang, L.; Saavedra, S. S. *Anal. Chem.* **1995**, *67*, 1307–1314.
(51) Grummt, U. W.; Pron, A.; Zagorska, M.; Lefrant, S. *Anal. Chim. Acta* **1997**, *357*, 253–259.
(52) Vonklitzing, R.; Mohwald, H. *Langmuir* **1995**, *11*, 3554–3559.
(53) Ge, C.; Doherty, W. J., III; Mendes, S. B.; Armstrong, N. R.; Saavedra, S. S. *Talanta* **2005**, *65*, 1126–1131.
(54) Bradshaw, J. T.; Mendes, S. B.; Armstrong, N. R.; Saavedra, S. S. *Anal. Chem.* **2003**, *75*, 1080–1088.
(55) Reimhult, E.; Hook, F.; Kasemo, B. *Langmuir* **2003**, *19*, 1681–1691.
(56) Seu, K. J.; Pandey, A. P.; Haque, F.; Proctor, E. A.; Ribbe, A. E.; Hovis, J. S. *Biophys. J.* **2007**, *92*, 2445–2450.
(57) Hamai, C.; Yang, T. L.; Kataoka, S.; Cremer, P. S.; Musser, S. M. *Biophys. J.* **2006**, *90*, 1241–1248.
(58) Grzesiek, S.; Dencher, N. A. *Biophys. J.* **1986**, *50*, 265–276.
(59) Deamer, D. W. *J. Bioenerg. Biomembr.* **1987**, *19*, 457–479.
(60) Nichols, J. W.; Deamer, D. W. *Proc. Natl. Acad. Sci. U. S. A.* **1980**, *77*, 2038–2042.
(61) Henderso., Pj; McGivan, J. D.; Chappell, J. B. *Biochem. J.* **1969**, *111*, 521–&.
(62) Ahmed, I.; Krishnamoorthy, G. *Biochim. Biophys. Acta* **1990**, *1024*, 298–306.
(63) Yamaguchi, A.; Anraku, Y. *Biochim. Biophys. Acta* **1978**, *501*, 136–149.
(64) Prabhananda, B. S.; Kombrabail, M. H. *Biochim. Biophys. Acta, Biomembr.* **1995**, *1235*, 323–335.
(65) Kasianowicz, J.; Benz, R.; McLaughlin, S. *J. Membr. Biol.* **1984**, *82*, 179–190.
(66) Leblanc, O. H. *J. Membr. Biol.* **1971**, *4*, 227–251.
(67) Deamer, D. W.; Nichols, J. W. *Proc. Natl. Acad. Sci. U. S. A.* **1983**, *80*, 165–168.